Systematic and Accurate Method to Model Dielectric Stratifications in Artificial Dielectric Layers

Tapia Barroso, Roderick G.; Cavallo, Daniele

DOI
10.1109/TAP.2025.3529196

Publication date
2025

Document Version
Final published version

Published in
IEEE Transactions on Antennas and Propagation

Communication

Systematic and Accurate Method to Model Dielectric Stratifications in Artificial Dielectric Layers

Roderick G. Tapia Barroso and Daniele Cavallo

***Abstract*— We present a systematic approach to include the effects of dielectric slabs in artificial dielectric layers (ADLs). Typical implementations of ADLs consist of layers of subwavelength metal patches supported by either dielectric slabs or thin dielectric films bonded onto foam spacers. The presence of dielectrics in the proximity of the metal layers affects the equivalent layer capacitance and thus must be accurately taken into account for the modeling and design of the ADLs. The proposed procedure allows to derive an analytical expression for the effective permittivity of each capacitive layer that depends on the dielectric layers in the vicinity of the metal. The equivalent layer capacitance can then be included in the ADL equivalent transmission line model, which can be used, for instance, for the design of matching structures in ultrawideband arrays.**

***Index Terms*— Artificial dielectric layers (ADLs), effective permittivity, spectral domain method, stratified media, wideband arrays.**

I. Introduction

Artificial dielectric layers (ADLs) are commonly adopted structures in the design of lenses, antennas, and arrays. They consist of a number of capacitive metal meshes typically made of subwavelength periodic patches [1], [2]. Their effective electric and magnetic properties can be engineered by controlling the spatial density of the metal patches, i.e., the period and the size of the patches, as well as the distance and the mutual shift between layers. ADLs have been used to design microwave or millimeter-wave lenses [2], [3], as partially reflective surfaces in leaky-wave antennas [4], and as wide-angle impedance matching layers in antenna arrays [5]. A specific application considered in this communication is the use of ADLs as superstrates in ultrawideband array designs [6], [7].

The design of ADLs exploits the availability of equivalent circuits that describe the propagation of a plane wave through the material by means of transmission lines in which each metal layer is represented as an equivalent shunt capacitance.

Closed-form expressions for the layer capacitance of a single layer were derived in [8], [9], [10], [11], [12], and [13]. Floquet analyses to derive the equivalent capacitance of periodic strips or circular patches were given in [14] and [15], but only for free-space case. The solution given in [13] is particularly advantageous for its simple generalization to the case of multilayer ADLs. When the distance between layers is small compared with the period, it is important to account for the reactive coupling between layers in the estimation of the capacitance. A closed-form capacitance formula that accounts for the interaction between layers was derived in [16], which is valid for general structures where each layer can have different geometrical parameters.

One key advantage of ADLs when used as slabs in antenna and array designs is that they exhibit anisotropic properties, i.e., their effective refractive index decreases with the incidence angle. This characteristic behavior allows to avoid the excitation of surface waves. To maximize the anisotropy, the optimal hosting medium of ADLs is free space. However, physical realization of ADLs requires dielectric slabs to support the patches. Previous implementations considered patches printed on very thin dielectric films glued to foam spacers [7], [17], to emulate the ideal free-space hosting medium. However, the thin dielectric substrates and bonding layers change the effective capacitance of the metal layer. This effect was never rigorously included in previous models.

Some techniques to estimate the effective permittivity of a layer in the presence of dielectrics are used in [10], [11], and [12], but they are only accurate for dielectric thickness that is much larger than the gap between patches. Contrarily, for very thin dielectric layers, a method was proposed in [18] to estimate the effective capacitance and consisted in studying the propagation along a slotline with width equal to the gap between patches and embedded in the same dielectric stratification as the ADLs. However, this method is not rigorous and its accuracy is greatly varying depending on the specific ADL design.

In this communication, we propose a systematic approach to include the effects of dielectric slabs with arbitrary thickness. The procedure allows to derive a closed-form expression for the effective permittivity of each capacitive layer that depends on the dielectrics in the vicinity of the metal. We resort to spectral domain methods to study scattering from a single layer, with and without the dielectrics. By comparison of these two results, we derive an effective permittivity that is used as a correction factor for the layer capacitance. The expressions are valid for both transverse electric (TE) and transverse magnetic (TM) modes and for general oblique incidence.

The equivalent layer capacitance can then be included in the equivalent transmission line model in a multilayer configuration. A validation of the method is presented, based on the use of ADLs as matching structures for ultrawideband arrays. As an example of application, we use our model for the estimation of the active reflection coefficient of connected arrays loaded with ADLs.

II. Analysis of a Single Layer

A single layer of an ADL structure is a capacitive mesh, made of periodic square metal patches. It is assumed that both the patch size and the period are subwavelength ($<\lambda/4$) and that the patches are infinitely thin and perfectly conducting. It is well-known that the scattering from such a layer is azimuthally independent [19], thus we can assume, without loss of generality, that the plane of incidence is $\phi = 0°$, aligned with one of the two orthogonal gaps between patches [see Fig. 1(a)].

A. Free Space

To explain the method used for the analysis of ADLs in general dielectric stratified media, we start from the known solution of a single layer in free space, under generic plane-wave incidence from the direction θ [Fig. 1(a)]. The layer consists of periodic patches

Received 1 October 2024; revised 4 December 2024; accepted 30 December 2024. Date of publication 20 January 2025; date of current version 9 April 2025. *(Corresponding author: Roderick G. Tapia Barroso.)*

The authors are with the Microelectronics Department, Delft University of Technology, 2628 CD Delft, The Netherlands (e-mail: r.g.tapiabarroso@tudelft.nl; d.cavallo@tudelft.nl).

Digital Object Identifier 10.1109/TAP.2025.3529196

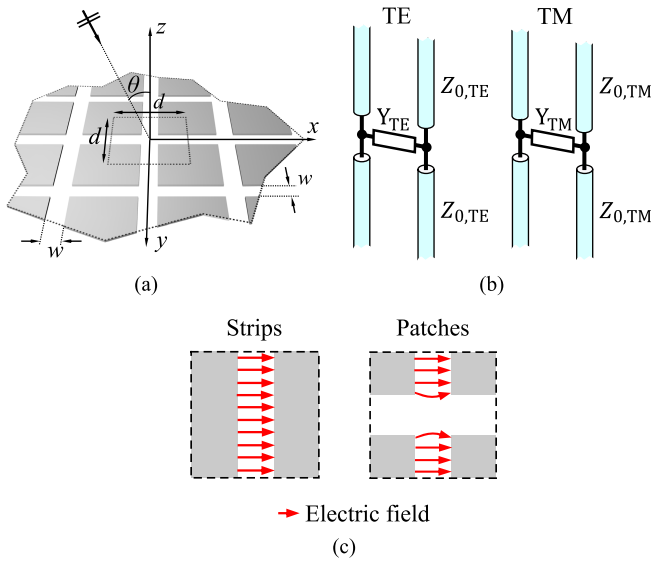

Fig. 1. (a) Single layer of subwavelength periodic square patches in free space under generic plane-wave illumination. (b) Equivalent transmission line model for TE and TM incidences. (c) Electric field in the gaps for periodic strips and patches, explaining the correction factor α for the edge capacitance.

with spacing d and gap width w. A method was described in [13], based on a spectral method of moments (MoM) analysis, leading through some approximations to the equivalent circuit representation in Fig. 1(b). This equivalent circuit consists of two transmission lines representing the fundamental Floquet wave, for the TE and TM modes, respectively. The lines have characteristic impedance $Z_{0,\mathrm{TM}} = \zeta_0 k_{z0}/k_0$ and $Z_{0,\mathrm{TE}} = \zeta_0 k_0/k_{z0}$, where k_0 and ζ_0 are the free-space wavenumber and impedance, and $k_{z0} = k_0 \cos\theta$ is the propagation constant on the lines.

The layer equivalent admittances for TE and TM waves are given by

$$Y_{\mathrm{TM}} = jB_{\mathrm{FS}} \tag{1}$$

$$Y_{\mathrm{TE}} = jB_{\mathrm{FS}}\left(1 - \frac{k_{\rho 0}^2}{2k_0^2}\right) \tag{2}$$

where $k_{\rho 0} = k_0 \sin\theta$. The admittances are expressed in terms of the free-space layer susceptance B_{FS}, defined as

$$B_{\mathrm{FS}} = \alpha \frac{\omega \varepsilon_0 d}{\pi} \sum_{m_x \neq 0} \frac{1}{|m_x|} \mathrm{sinc}^2\left(\frac{\pi m_x w}{d}\right) \tag{3}$$

where ω is the angular frequency, ε_0 is the vacuum permittivity, and m_x is an integer that denotes the index of the Floquet mode. We introduced the factor α that is equal to $(d - w)/d$. This factor takes into account the difference in capacitance between strips and patches, when the phase of the electric field in the gaps is uniform [see Fig. 1(c)].

B. General Dielectric Stratification: MoM Solution

The expressions given in the previous section are only valid for a layer in free space. To derive an expression for the layer admittance in arbitrary stratified media, we have to recall the general MoM solution given in [13] and [20]. The procedure consisted of solving for the equivalent magnetic current in the gaps by defining four entire domain basis functions. Two basis functions are constant in amplitude and linear in phase to account for the oblique incidence, as shown in Fig. 2(a). The other two functions are odd distributions [see Fig. 2(b)] needed to represent the continuity of the field at the crossing between slots.

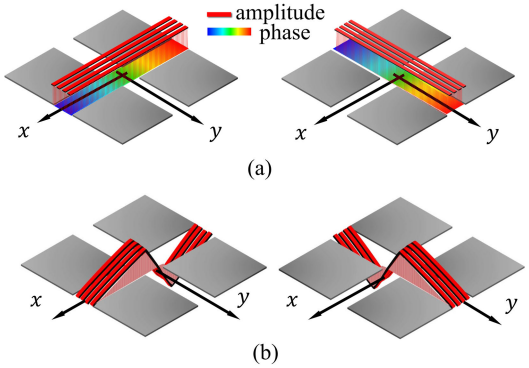

Fig. 2. Representation of (a) linear phase basis functions and (b) odd basis functions.

The elements of the 4×4 MoM admittance matrix can be expressed in the spectral domain as

$$Y_{pq} = -\frac{1}{d^2} \sum_{m_x=-\infty}^{\infty} \sum_{m_y=-\infty}^{\infty} \mathbf{F}_p\left(k_{xm}, k_{ym}\right) \mathbf{G}\left(k_{xm}, k_{ym}\right) \cdot \mathbf{F}_q^*\left(-k_{xm}, -k_{ym}\right) \tag{4}$$

where $k_{xm} = k_{x0} - (2\pi m_x)/d$ and $k_{ym} = -(2\pi m_y)/d$ are the Floquet modes, with $k_{x0} = k_0 \sin\theta$, and the symbol $*$ denotes complex conjugation. $\mathbf{G}$ is the dyadic spectral Green's function relating magnetic field to magnetic source, and $\mathbf{F}_p$ and $\mathbf{F}_q$ are the Fourier transforms of the basis and test functions, respectively, and are given explicitly in the Appendix.

Following the steps in the Appendix, the TE and TM components of the admittance matrix can be written as

$$Y_{\mathrm{TMTM}} = Y_{22} \tag{5}$$

$$Y_{\mathrm{TETE}} = Y_{11} - \frac{Y_{41}Y_{14}Y_{33}}{Y_{33}Y_{44} - Y_{34}Y_{43}}. \tag{6}$$

The approximated expressions of all the mutual admittance terms are given in (21)–(27). To arrive to a circuit representation, it is convenient to split the admittances in a term accounting for the fundamental Floquet wave Y_{f} and a term including all higher order modes Y_{ho}

$$Y_{\mathrm{TMTM}} = Y_{\mathrm{f,TM}} + Y_{\mathrm{ho,TM}} \tag{7}$$

$$Y_{\mathrm{TETE}} = Y_{\mathrm{f,TE}} + Y_{\mathrm{ho,TE}}. \tag{8}$$

The fundamental Floquet mode can be approximated as the xx- and yy-components of the spectral dyadic Green's function [13]

$$Y_{\mathrm{f,TM}} = -G_{yy}\left(k_{x0}, 0\right) \tag{9}$$

$$Y_{\mathrm{f,TE}} = -G_{xx}\left(k_{x0}, 0\right) \tag{10}$$

while the higher order terms are

$$Y_{\mathrm{ho,TM}} = -\sum_{m_x \neq 0} S_{m_x} G_{yy}\left(k_{xm}, 0\right) \tag{11}$$

$$Y_{\mathrm{ho,TE}} = -\sum_{m_y \neq 0} S_{m_y} G_{xx}\left(k_{x0}, k_{ym}\right) - \frac{Y_{41}Y_{14}Y_{33}}{Y_{33}Y_{44} - Y_{34}Y_{43}} \tag{12}$$

where $S_{m_x} = \mathrm{sinc}^2(k_{xm} w/2)$ and $S_{m_y} = \mathrm{sinc}^2(k_{ym} w/2)$.

The expressions (5) to (12) can be applied to arbitrary dielectric stratification, since they are written in terms of the spectral Green's function, which is known for layered media by solving an equivalent transmission line problem (see the Appendix). Therefore, the fundamental mode can be modeled as equivalent transmission line sections representing the stratified medium, while the higher order modes are

described as a shunt admittance, which also takes into account the presence of the dielectrics through Green's function.

C. General Dielectric Stratification: Approximated Solution

While the expressions (5)–(12) can be used to find the equivalent layer admittance for arbitrary oblique incidence and general dielectric stratification, they still require several Floquet sums to be computed for each incidence angle. Furthermore, these solutions do not allow to easily extend the method to multiple layers. For this reason, in this section we propose an approximated formula for the layer admittance that is simpler to compute and can be directly applied for multilayer configurations.

We start from the assumption that the layer admittance in the presence of dielectrics can be related to the free-space admittance in (1) and (2) as follows:

$$Y_{\mathrm{TM}} = j\varepsilon_{r,\mathrm{eff}} B_{\mathrm{FS}} \tag{13}$$

$$Y_{\mathrm{TE}} = j\varepsilon_{r,\mathrm{eff}} B_{\mathrm{FS}} \left(1 - \frac{k_{\rho 0}^2}{2k_0^2 \varepsilon_{r,\mathrm{eff}}}\right) \tag{14}$$

where the effective layer permittivity $\varepsilon_{r,\mathrm{eff}}$ is introduced, multiplying the susceptance in both Y_{TM} and Y_{TE}, and the wavenumber in Y_{TE}. This assumption was also used in [10] and [12]. However, accurate estimation of $\varepsilon_{r,\mathrm{eff}}$ has only been available for simple stratifications, i.e., when the metal patches are immersed in an infinite homogeneous medium or at the boundary of two infinitely extending homogeneous media. On the contrary, the method presented here is valid for a more general dielectric stratification.

The expression in (14) assumes that $\varepsilon_{r,\mathrm{eff}}$ is not varying with the angle of incidence. Under this hypothesis, $\varepsilon_{r,\mathrm{eff}}$ can be calculated for normal incidence, by comparing (11) with (1) and (3), leading to

$$\varepsilon_{r,\mathrm{eff}} \approx \frac{-\sum_{m_x \neq 0} S_{m_x} G_{yy}(k_{xm}, 0)}{j\omega\varepsilon_0 d/\pi \sum_{m_x \neq 0} S_{m_x}/|m_x|}. \tag{15}$$

It can be noted that even if the effective permittivity is derived for normal incidence, the dependence on the incidence angle is taken into account for TE incidence by the $k_{\rho 0}$ term in (14). To quantify the accuracy of the approximation (15), in Section III we compare it with the general MoM solution and CST simulations.

D. Example: Two Homogeneous Dielectrics

As an example, we consider a layer at the interface between two infinite media with relative permittivity, wavenumber, and impedance $\varepsilon_{r,1}$, k_1, ζ_1 and $\varepsilon_{r,2}$, k_2, ζ_2, respectively. Considering TM incidence at $\phi = 0$ Green's function is given as

$$\begin{aligned} G_{yy}(k_{xm}, 0) &= \frac{-k_1}{\zeta_1 \sqrt{k_1^2 - k_{xm}^2}} + \frac{-k_2}{\zeta_2 \sqrt{k_2^2 - k_{xm}^2}} \\ &\approx -\left(\frac{k_1}{\zeta_1} + \frac{k_2}{\zeta_2}\right) \frac{jd}{2\pi |m_x|} \end{aligned} \tag{16}$$

where we used the approximation $(k_i^2 - k_{xm}^2)^{1/2} \approx (-k_{xm}^2)^{1/2} \approx -j2\pi|m_x|/d$, with $i \in \{1, 2\}$, valid for the subwavelength period. Realizing that $k_i/\zeta_i = \omega\varepsilon_0\varepsilon_{r,i}$ and substituting (16) in (15), one obtains the well-known approximation

$$\varepsilon_{r,\mathrm{eff}} = \frac{\varepsilon_{r,1} + \varepsilon_{r,2}}{2}. \tag{17}$$

This average value is typically used as an approximation if the thickness of the two media is finite, yet large compared with the gaps w. To investigate how the effective permittivity of finite height slabs tends to the quasi-static approximation in (17), we study a layer of patches with period $d = 6$ mm, between two dielectric slabs with increasing but finite height h, and relative permittivities $\varepsilon_{r,1} = 3.4$ and $\varepsilon_{r,1} = 2.32$ as shown in Fig. 3(a). The $\varepsilon_{r,\mathrm{eff}}$ is plotted as a function of h for three different values of the width w. It can be seen that $\varepsilon_{r,\mathrm{eff}}$ in Fig. 3(b) converges faster to the quasi-static value in (17) for larger h/w ratios. However, the convergence is reached only for values of h large enough (around $d/4$).

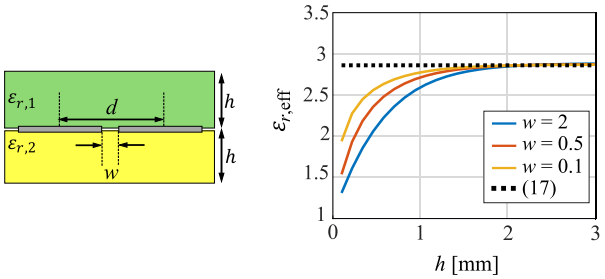

(a) (b)

Fig. 3. (a) Example of stratification, considering periodic patches between two slabs with height h and relative permittivities $\varepsilon_{r,1} = 3.4$ and $\varepsilon_{r,2} = 2.32$. (b) Effective permittivity as a function of h for different gap widths w.

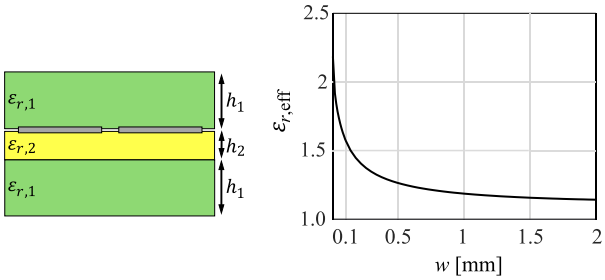

(a) (b)

Fig. 4. (a) Example of stratification, considering periodic patches with spacing $d = 6$ mm printed on a dielectric film with thickness $h_2 = 25\,\mu$m and relative permittivity $\varepsilon_{r,2} = 2.32$, and bonding layers above and below with thickness $h_1 = 38\,\mu$m and relative permittivity $\varepsilon_{r,1} = 3.4$. (b) Effective permittivity as a function of the gap width w.

III. Numerical Results

A. Single Layer

As an example, we consider a layer in the presence of a realistic dielectric stratification, as shown in Fig. 4(a). The patches are printed on a 25-μm-thick dielectric film with relative permittivity 2.32 and bonding layers are considered above and below with thickness 38 μm and relative permittivity 3.4.

The effective permittivity from (15) is evaluated and plotted in Fig. 4(b) as a function of the gap width w. Once the permittivity is calculated, the equivalent layer admittances are found using (13) and (14). The equivalent admittances of the metal patches can be placed in parallel to the TE and TM transmission lines representing the fundamental Floquet wave, as depicted in Fig. 5. The reflection coefficient for generic plane-wave incidence can then be found from the equivalent transmission lines.

To validate the method, we compare in Fig. 6 our analytical solution with CST simulations. Fig. 6(a) refers to a layer with period $d = 6$ mm and varying gap width w, at the calculation frequency of 5 GHz, under normal plane-wave incidence. A good comparison can be observed with CST, for both the cases with and without dielectrics. It can be noted that higher reflection occurs in the presence of the dielectrics, since the effective layer capacitance increases when the dielectrics are included. Fig. 6(b) shows the case for 60° TE and TM incidences, in the presence of the dielectric slabs. The expression for the layer impedance in (13)–(15) can be compared with more general expressions (9)–(12), to verify whether the assumption that

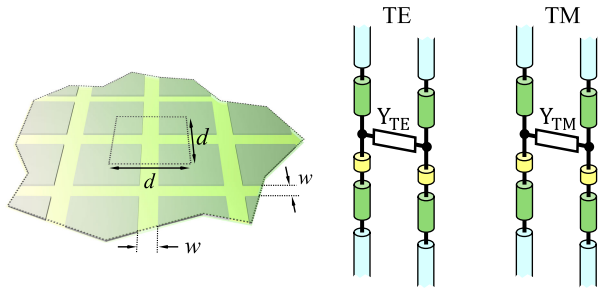

Fig. 5. Single layer of subwavelength periodic square patches in the presence of bonding layers. (a) Three-dimensional view. (b) Side view. (c) Equivalent TE/TM transmission lines.

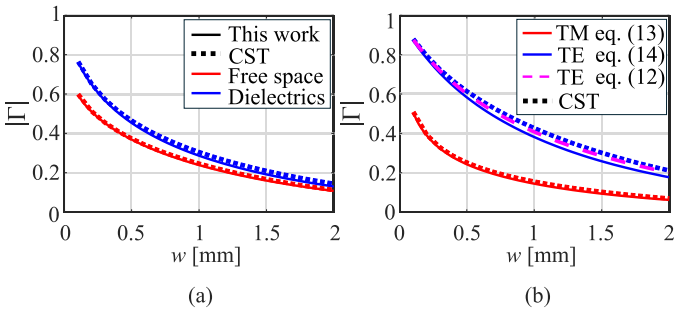

Fig. 6. Magnitude of the reflection coefficient for a layer with $d = 6$ mm and varying gap width w, at the calculation frequency of 5 GHz. Comparison between our method and CST is shown for (a) normal incidence, with and without dielectrics. (b) 60° TE and TM incidences, with dielectrics.

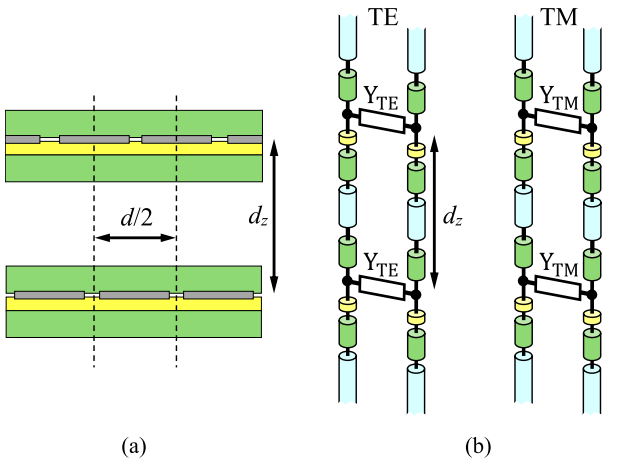

Fig. 7. Two-layer structure at distance d_z. (a) Side view and (b) equivalent transmission line. The two layers are shifted relative to each other so that the distance between the patch centers of the two layers is $d/2$.

$\varepsilon_{r,\text{eff}}$ is independent of the incidence angle is accurate. Both the MoM solution and the approximation based on the effective permittivity (computed for normal incidence) are in good agreement with CST.

B. Multiple Layers

Although the expression for the effective permittivity has been derived for a single layer, we can assess its validity in a multilayer ADL configuration. In multilayer ADLs, we use a more general expression of the layer susceptance B_{ML} given in [16], which accounts for the reactive coupling between layers. As such, the expression of the layer susceptance depends on the geometrical parameters of the layer itself, as well as on the geometries of the two adjacent layers above and below.

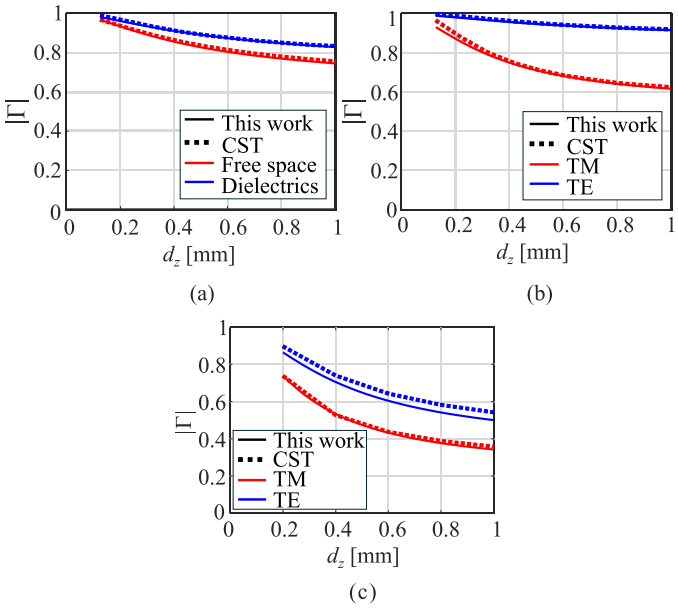

Fig. 8. Magnitude of the reflection coefficient for a two-layer structure with $d = 6$ mm and varying layer distance d_z, at the calculation frequency of 5 GHz. Comparison between our method and CST is shown for (a) normal incidence, with and without dielectrics, for $w = 0.3$ mm; (b) 60° TE and TM incidences, with dielectrics, for $w = 0.3$ mm; and (c) 45° TE and TM incidences, with dielectrics, for $w = 1.5$ mm.

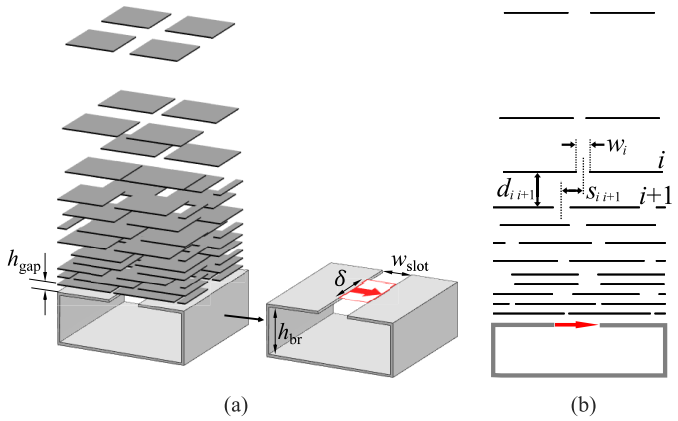

Fig. 9. (a) Three-dimensional view and (b) side view of the connected array unit cell with characteristic dimensions.

When dielectrics are included, we assume that this susceptance B_{ML} is multiplied by the effective permittivity derived for the single layer. To analyze the accuracy of this approximation, we consider two metal layers each surrounded by dielectrics with the same dimensions used for the single-layer analysis. The two metal layers are assumed to be at a distance d_z, shifted relative to each other so that the distance between the patch centers of the two layers is half the period ($d/2$), as depicted in Fig. 7(a). The equivalent transmission line in Fig. 7(b) can be used to estimate the reflection coefficient under generic oblique incidence.

The magnitude of the reflection coefficient for the two-layer structure with $d = 6$ mm, $w = 0.3$ mm, and varying layer distance d_z is shown at the frequency of 5 GHz in Fig. 8(a) and (b), for normal incidence and 60° incidence, respectively. Comparison between our method and CST is shown to be good in both the cases. The results for 45° incidence and a larger width $w = 1.5$ mm are presented in Fig. 8(c). The error with respect to CST is slightly worse in this case but still relatively small.

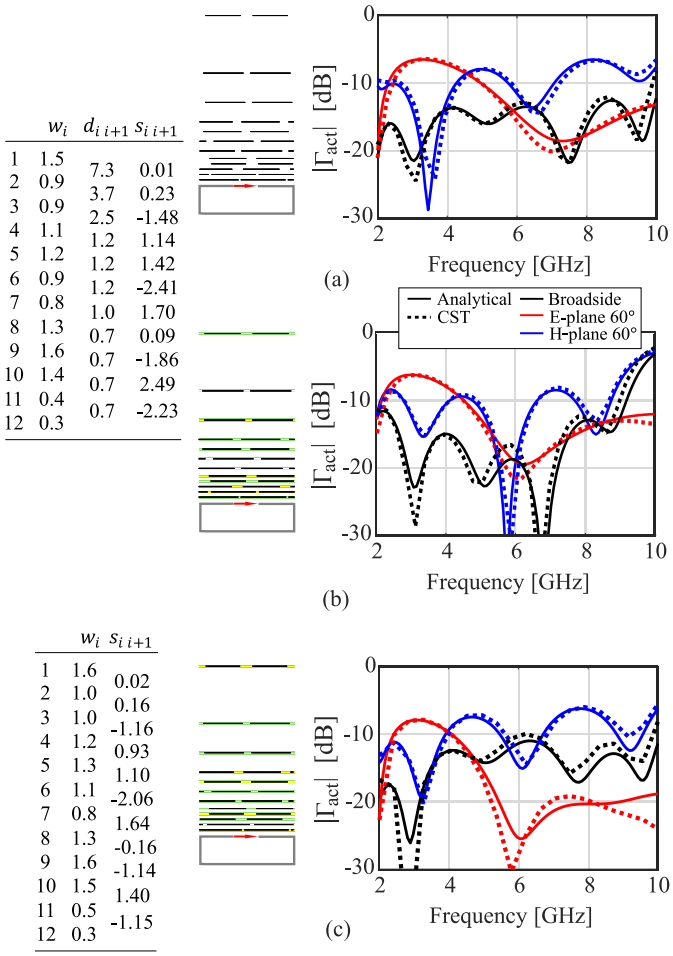

Fig. 10. Side view of the connected array unit cell with geometrical parameters (in mm) and active reflection coefficient. (a) Dimensions are optimized for free space. (b) Same dimensions as free space, but including the dielectrics. (c) Dimensions reoptimized by accounting for the dielectrics.

C. Application to Wideband Array Designs

As final validation of the method, we apply the proposed approach to the design of ADL superstrates for ultrawideband arrays. ADLs have been used in combination with connected slot elements to achieve wideband wide-scanning phased arrays [7], [17]. When considering multiple nonaligned layers with small interlayer distance, the factor α introduced in (3) is taken equal to 1 for H-plane scanning, since we observed a reduction in the effect illustrated in Fig. 1(c).

The active reflection coefficient of the unit cell can be evaluated with closed-form expressions that use the transmission line representation of ADLs. An example design with the 5:1 bandwidth is shown in Fig. 9(a), where the geometrical parameters of the connected array are as follows: $h_{\text{gap}} = 0.84$ mm, $h_{\text{br}} = 3.46$ mm, $\delta = 5$ mm, $w_{\text{slot}} = 3.07$ mm, and array spacing is 12 mm. The characteristic dimensions of the ADL are illustrated in Fig. 9(b), where w_i is the gap width between patches for the ith layer, while $d_{i\,i+1}$ and $s_{i\,i+1}$ are the distance and the shift between two adjacent layers with index i and $i+1$, respectively. This 12-layer ADL in free space is optimized to achieve the performance shown in Fig. 10(a), of which the geometrical parameters are given in the inset. Both the connected array input impedance formulas and CST show similar results, for broadside and scanning to 60° in the main planes.

If dielectrics are added for each layer without changing the ADL geometrical parameters, the active reflection coefficient performance degrades above 9 GHz as shown in Fig. 10(b). However, if we reoptimize the widths and shifts of the ADL using the modified formulas for the effective layer capacitance in the presence of the dielectrics, a new unit cell is obtained which achieves the performance shown in Fig. 10(c). Even for the example with large number of layers, the proposed method shows good comparison with full-wave simulations performed with CST. It can be emphasized that our method can simulate the unit cell in Fig. 9(b) in a few seconds, while CST simulations require several hours.

IV. Conclusion

We derived an analytical solution to take into account the effect of dielectric slabs in ADLs. Typical ADL designs for wideband arrays include electrically thin dielectric layers within the structure that change significantly the ADL performance with respect to free space. The method described here allows to accurately consider this effect, enabling the efficient optimization of the array unit cell performance in the presence of realistic dielectric stacks.

Appendix
Derivation of Admittance Matrix Elements

The MoM solution for a single layer involves the calculation of mutual admittances defined in (4). The admittances are written as spectral domain Floquet sums, in terms of the Fourier transform of the basis functions

$$\begin{aligned} F_1\left(k_{xm}, k_{ym}\right) &= d\delta\left(m_x\right)\operatorname{sinc}\left(k_{ym}w/2\right) \\ F_2\left(k_{xm}, k_{ym}\right) &= d\delta\left(m_y\right)\operatorname{sinc}\left(k_{xm}w/2\right) \\ F_3\left(k_{xm}, k_{ym}\right) &= B_d\left(k_{xm}\right)\operatorname{sinc}\left(k_{ym}w/2\right) \\ F_4\left(k_{xm}, k_{ym}\right) &= B_d\left(k_{ym}\right)\operatorname{sinc}\left(k_{xm}w/2\right) \end{aligned} \tag{18}$$

where $\delta(\cdot)$ is the Kronecker delta, and the function B_d is the Fourier transform of the odd distribution depicted in Fig. 2(b)

$$\begin{aligned} &B_d(k_x) \\ &= \frac{e^{-j(k_x+k_0)\frac{d}{2}} - e^{-j(k_x+k_0)\frac{w}{2}}}{j\left(k_x+k_0\right)} - \Gamma\frac{e^{-j(k_x-k_0)\frac{w}{2}} - e^{-j(k_x-k_0)\frac{d}{2}}}{j\left(k_x-k_0\right)} \\ &\quad + \frac{e^{j(k_x-k_0)\frac{d}{2}} - e^{j(k_x-k_0)\frac{w}{2}}}{j\left(k_x-k_0\right)} + \Gamma\frac{e^{j(k_x+k_0)\frac{d}{2}} - e^{j(k_x+k_0)\frac{w}{2}}}{j\left(k_x+k_0\right)} \\ &\quad + C\frac{k_x w\cos\left(k_x w/2\right) - 2\sin\left(k_x w/2\right)}{jk_x^2} \end{aligned} \tag{19}$$

with $\Gamma = -e^{-jk_0 d}$ and $C = 2/w(e^{-jk_0(w/2)} + \Gamma e^{jk_0(w/2)})$.

The admittance matrix can be simplified by noting that $Y_{13} \approx Y_{31} \approx Y_{24} \approx Y_{42} \approx 0$ as they represent the projection of a nearly uniform basis function onto an odd function. Without loss of generality, we may assume that similar to the free-space case the reduced admittance matrix is azimuthally independent, and thus the analysis can be continued by assuming $\phi = 0°$. The reduced admittance matrix for TE and TM modes is diagonal (TE and TM modes are decoupled) and given as follows:

$$\begin{bmatrix} Y_{\text{TMTM}} & 0 \\ 0 & Y_{\text{TETE}} \end{bmatrix} = \begin{bmatrix} Y_{22} & 0 \\ 0 & Y_{11} - \dfrac{Y_{41}Y_{14}Y_{33}}{Y_{33}Y_{44} - Y_{34}Y_{43}} \end{bmatrix}. \tag{20}$$

We now calculate the matrix elements explicitly as

$$Y_{22} = -\sum_{m_x=-\infty}^{\infty} S_{m_x} G_{yy}\left(k_{xm}, k_{y0}\right) \tag{21}$$

$$Y_{11} = -\sum_{m_y=-\infty}^{\infty} S_{m_y} G_{xx}\left(k_{x0}, k_{ym}\right) \tag{22}$$

$$Y_{14} \approx -\frac{jwC}{d_y}\sum_{m_y\neq 0}\frac{S_{m_y}}{k_{ym}} G_{xy}\left(k_{x0}, k_{ym}\right) \tag{23}$$

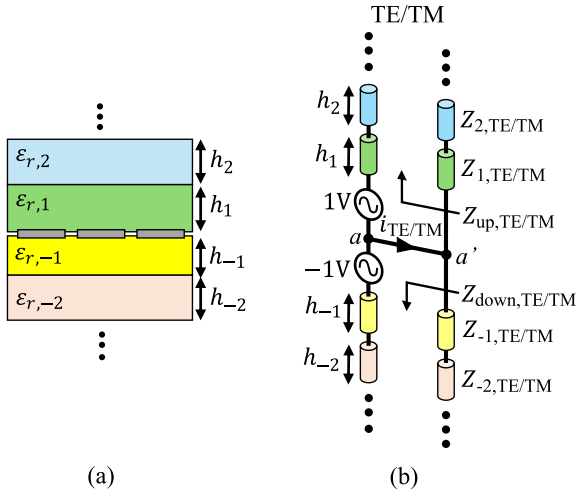

Fig. 11. (a) Layer embedded in general stratified medium and (b) equivalent transmission lines to evaluate spectral Green's function.

$$Y_{44} \approx \frac{1}{d_x}\frac{1}{d_y}|jwC|^2 \sum_{m_x=-\infty}^{\infty} \sum_{m_y\neq 0} \frac{S_{m_y} S_{m_x}}{k_{ym}^2} G_{yy}\left(k_{xm}, k_{ym}\right) \quad (24)$$

$$Y_{33} \approx \frac{1}{d_x}\frac{1}{d_y}|jwC|^2 \sum_{m_x\neq 0} \sum_{m_y=-\infty}^{\infty} \frac{S_{m_y} S_{m_x}}{k_{xm}^2} G_{xx}\left(k_{xm}, k_{ym}\right) \quad (25)$$

$$Y_{34} \approx \frac{1}{d_x}\frac{1}{d_y}|jwC|^2 \sum_{m_x\neq 0} \sum_{m_y\neq 0} \frac{S_{m_y} S_{m_x}}{k_{ym} k_{xm}} G_{xy}\left(k_{xm}, k_{ym}\right) \quad (26)$$

$$Y_{43} \approx Y_{34}. \quad (27)$$

To obtain the components of the dyadic Green's function, one can solve for the currents i_{TE} and i_{TM} on the TE and TM transmission lines representing the generic layered medium above and below the metal layer, as shown in Fig. 11. The line sections of the ith slab have characteristic impedance $Z_{i,\mathrm{TM}} = \zeta_i k_{zi}/k_i$ and $Z_{i,\mathrm{TE}} = \zeta_i k_i/k_{zi}$, where k_i and ζ_i are the wavenumber and impedance of the medium, and k_{zi} is the propagation constant on the line sections.

Assuming magnetic currents and magnetic fields only oriented along x and y, the relevant components of the dyadic Green's function are given by

$$\begin{bmatrix} G_{xx}(k_x,k_y) & G_{xy}(k_x,k_y) \\ G_{yx}(k_x,k_y) & G_{yy}(k_x,k_y) \end{bmatrix} = \begin{bmatrix} -\dfrac{i_{\mathrm{TE}}k_x^2 + i_{\mathrm{TM}}k_y^2}{k_\rho^2} & \dfrac{(i_{\mathrm{TM}} - i_{\mathrm{TE}})\,k_x k_y}{k_\rho^2} \\ \dfrac{(i_{\mathrm{TM}} - i_{\mathrm{TE}})\,k_x k_y}{k_\rho^2} & -\dfrac{i_{\mathrm{TM}}k_x^2 + i_{\mathrm{TE}}k_y^2}{k_\rho^2} \end{bmatrix} \quad (28)$$

where $k_\rho^2 = k_x^2 + k_y^2$. From Fig. 11(b), the currents flowing through the short-circuit at the aa' terminals can be found as the parallel of the input impedances for the upper and lower lines

$$i_{\mathrm{TE}} = \frac{1}{Z_{\mathrm{up,TE}}} + \frac{1}{Z_{\mathrm{down,TE}}} \quad (29)$$

$$i_{\mathrm{TM}} = \frac{1}{Z_{\mathrm{up,TM}}} + \frac{1}{Z_{\mathrm{down,TM}}}. \quad (30)$$

REFERENCES

[1] W. E. Kock, "Metallic delay lenses," *Bell Syst. Tech. J.*, vol. 27, no. 1, pp. 58–82, Jan. 1948.

[2] S. S. D. Jones and J. Brown, "Metallic delay lenses," *Nature*, vol. 163, no. 4139, pp. 324–325, Feb. 1949.

[3] C. M. Coco Martin, W. Hu, and D. Cavallo, "Design of wideband flat artificial dielectric lenses at mmWave frequencies," *IEEE Trans. Antennas Propag.*, vol. 72, no. 2, pp. 1418–1428, Feb. 2024.

[4] A. P. Feresidis, G. Goussetis, S. Wang, and J. C. Vardaxoglou, "Artificial magnetic conductor surfaces and their application to low-profile high-gain planar antennas," *IEEE Trans. Antennas Propag.*, vol. 53, no. 1, pp. 209–215, Jan. 2005.

[5] M. Soltani and G. V. Eleftheriades, "Wide-angle impedance matching of a patch antenna phased array using artificial dielectric sheets," *IEEE Trans. Antennas Propag.*, vol. 72, no. 5, pp. 4258–4270, May 2024.

[6] D. Cavallo, "Recent advances on wideband wide scanning connected slot arrays," in *Proc. IEEE Int. Symp. Phased Array Syst. Technol. (PAST)*, Waltham, MA, USA, Oct. 2022, pp. 1–3.

[7] R. Ozzola, A. Neto, U. Imberg, and D. Cavallo, "Connected slot array with interchangeable ADL radome for sub-8 GHz 5G applications," *IEEE Trans. Antennas Propag.*, vol. 72, no. 1, pp. 992–997, Jan. 2024.

[8] J. R. Wait, "Theories of scattering from wire-grid and mesh structures," in *Electromagnetic Scattering*, P. L. E. Uslenghi, Ed., New York, NY, USA: Academic, 1978, pp. 253–287.

[9] R. C. Compton and D. B. Rutledge, "Approximation techniques for planar periodic structures," *IEEE Trans. Microw. Theory Techn.*, vol. MTT-33, no. 10, pp. 1083–1088, Oct. 1985.

[10] O. Luukkonen et al., "Simple and accurate analytical model of planar grids and high-impedance surfaces comprising metal strips or patches," *IEEE Trans. Antennas Propag.*, vol. 56, no. 6, pp. 1624–1632, Jun. 2008.

[11] C. S. Kaipa, A. B. Yakovlev, F. Medina, F. Mesa, C. A. Butler, and A. P. Hibbins, "Circuit modeling of the transmissivity of stacked two-dimensional metallic meshes," *Opt. Exp.*, vol. 18, no. 13, pp. 13309–13320, 2010.

[12] L.B. Whitbourn and R. C. Compton, "Equivalent circuit formulas for metal grid reflectors at a dielectric boundary," *Appl. Opt.*, vol. 24, pp. 217–220, Jan. 1985.

[13] D. Cavallo, W. H. Syed, and A. Neto, "Closed-form analysis of artificial dielectric layers—Part I: Properties of a single layer under plane-wave incidence," *IEEE Trans. Antennas Propag.*, vol. 62, no. 12, pp. 6256–6264, Dec. 2014.

[14] N. Marcuvitz, *Waveguide Handbook*. New York, NY, USA: Institute of Electrical Engineers, 1986.

[15] R. E. Collin, *Field Theory Guided Waves*, 2nd ed., New York, NY, USA: IEEE Press, 1990.

[16] D. Cavallo and R. M. van Schelven, "Closed-form analysis of artificial dielectric layers with non-periodic characteristics," in *Proc. 13th Eur. Conf. Antennas Propag. (EuCAP)*, Krakow, Poland, Mar. 2019, pp. 1–5.

[17] D. Cavallo, W. H. Syed, and A. Neto, "Connected-slot array with artificial dielectrics: A 6 to 15 GHz dual-pol wide-scan prototype," *IEEE Trans. Antennas Propag.*, vol. 66, no. 6, pp. 3201–3206, Jun. 2018.

[18] A. J. van Katwijk, "Design of a wideband wide-scan connected slot array antenna using artificial dielectrics," M.S. thesis, EEMCS Faculty, Delft Univ. Technol., Delft, The Netherlands, 2019.

[19] S. A. Tretyakov, *Analytical Modelling in Applied Electromagnetics*. London, U.K.: Artech House, 2003.

[20] D. Cavallo and C. Felita, "Analytical formulas for artificial dielectrics with nonaligned layers," *IEEE Trans. Antennas Propag.*, vol. 65, no. 10, pp. 5303–5311, Oct. 2017.